PROCEEDINGS OF SPIE

Technical and scientific performance of the prototype Schwarzschild-Couder telescope for CTA

C. Adams, G. Ambrosi, M. Ambrosio, C. Aramo, P. Batista, et al.

Technical and scientific performance of the prototype Schwarzschild-Couder Telescope for CTA

C. B. Adams[1], G. Ambrosi[2], M. Ambrosio[3], C. Aramo[3], P. I. Batista[4], W. Benbow[5],
B. Bertucci[2,6], E. Bissaldi[7,8], M. Bitossi[9], A. Boiano[3], C. Bonavolontà[3,10], R. Bose[11], A. Brill[1],
A. M. Brown[12], J. H. Buckley[11], R. Canestrari[13], M. Capasso[14], M. Caprai[2], C. E. Covault[15],
D. Depaoli[16,17], L. Di Venere[7,8], M. Errando[11], S. Fegan[18], Q. Feng[14], E. Fiandrini[2,19],
A. Furniss[20], A. Gent[21], N. Giglietto[7,8], F. Giordano[7,8], E. Giro[22], R. Halliday[23], O. Hervet[24],
J. Holder[25], T. B. Humensky[26], S. Incardona[27,28], M. Ionica[2], W. Jin[29], D. Kieda[30],
F. Licciulli[8], S. Loporchio[7,8], G. Marsella[27,28], V. Masone[3], K. Meagher[21,31], T. Meures[31],
B. A. W. Mode[31], S. A. I. Mognet[32], R. Mukherjee[14], D. Nieto[33,34], A. Okumura[35], N. Otte[21],
F. R. Pantaleo[7,8], R. Paoletti[36,9], G. Pareschi[37], F. Di Pierro[17], E. Pueschel[4], D. Ribeiro[1],
L. Riitano[31], E. Roache[5], D. Ross[38], J. Rousselle[39], A. Rugliancich[9], M. Santander[29],
R. Shang[40], L. Stiaccini[36,9], H. Tajima[35], L. P. Taylor[31], L. Tosti[2], G. Tovmassian[41],
G. Tripodo[27,28], V. Vagelli[42,2], M. Valentino[10,3], J. Vandenbroucke[31], V. V. Vassiliev[40],
J. J. Watson[43], R. White[44], D. A. Williams[24], P. Yu[40], and A. Zink[45]

[1]Physics Department, Columbia University, New York, NY 10027, USA
[2]INFN Sezione di Perugia, 06123 Perugia, Italy
[3]INFN Sezione di Napoli, 80126 Napoli, Italy
[4]Deutsches Elektronen-Synchrotron, Platanenallee 6, 15738 Zeuthen, Germany
[5]Center for Astrophysics — Harvard & Smithsonian, Cambridge, MA 02138, USA
[6]Dipartimento di Fisica e Geologia dell'Università degli Studi di Perugia, 06123 Perugia, Italy
[7]Dipartimento Interateneo di Fisica dell'Università e del Politecnico di Bari, 70126 Bari, Italy
[8]INFN Sezione di Bari, 70125 Bari, Italy
[9]INFN Sezione di Pisa, 56127 Pisa, Italy
[10]CNR-ISASI, 80078 Pozzuoli, Italy
[11]Department of Physics, Washington University, St. Louis, MO 63130, USA
[12]Dept. of Physics and Centre for Advanced Instrumentation, Durham University, Durham
DH1 3LE, United Kingdom
[13]INAF IASF Palermo, 90146 Palermo, Italy
[14]Department of Physics and Astronomy, Barnard College, Columbia University, NY 10027,
USA
[15]Department of Physics, Case Western Reserve University, Cleveland, Ohio 44106, USA
[16]Dipartimento di Fisica dell'Università degli Studi di Torino, 10125 Torino, Italy
[17]INFN Sezione di Torino, 10125 Torino, Italy
[18]LLR/Ecole Polytechnique, Route de Saclay, 91128 Palaiseau Cedex, France
[19]Y
[20]Department of Physics, California State University - East Bay, Hayward, CA 94542, USA
[21]School of Physics & Center for Relativistic Astrophysics, Georgia Institute of Technology,
Atlanta, GA 30332-0430, USA
[22]INAF Osservatorio Astronomico di Padova, 35122 Padova, Italy
[23]Dept. of Physics and Astronomy, Michigan State University, East Lansing, MI 48824, USA
[24]Santa Cruz Institute for Particle Physics and Department of Physics, University of
California, Santa Cruz, CA 95064, USA

[25]Department of Physics and Astronomy and the Bartol Research Institute, University of Delaware, Newark, DE 19716, USA

[26]Science Department, SUNY Maritime College, Throggs Neck, NY 10465

[27]Dipartimento di Fisica e Chimica "E. Segrè", Università degli Studi di Palermo, via delle Scienze, 90128 Palermo, Italy

[28]INFN Sezione di Catania, 95123 Catania, Italy

[29]Department of Physics and Astronomy, University of Alabama, Tuscaloosa, AL 35487, USA

[30]Department of Physics and Astronomy, University of Utah, Salt Lake City, UT 84112, USA

[31]Department of Physics and Wisconsin IceCube Particle Astrophysics Center, University of Wisconsin, Madison, WI 53706, USA

[32]Pennsylvania State University, University Park, PA 16802, USA

[33]Institute of Particle and Cosmos Physics (IPARCOS), Universidad Complutense de Madrid, E-28040 Madrid, Spain

[34]Department of EMFTEL, Universidad Complutense de Madrid, E-28040 Madrid, Spain

[35]Institute for Space–Earth Environmental Research and Kobayashi–Maskawa Institute for the Origin of Particles and the Universe, Nagoya University, Nagoya 464-8601, Japan

[36]Dipartimento di Scienze Fisiche, della Terra e dell'Ambiente, Università degli Studi di Siena, 53100 Siena, Italy

[37]INAF - Osservatorio Astronomico di Brera, 20121 Milano/Merate, Italy

[38]Space Research Centre, University of Leicester, University Road, Leicester, LE1 7RH, United Kingdom

[39]Subaru Telescope NAOJ, Hilo HI 96720, USA

[40]Department of Physics and Astronomy, University of California, Los Angeles, CA 90095, USA

[41]Instituto de Astronomía, Universidad Nacional Autónoma de México, Ciudad de México, Mexico

[42]Agenzia Spaziale Italiana, 00133 Roma, Italy

[43]Deutsches Elektronen-Synchrotron, Platanenallee 6, D-15738 Zeuthen, Germany

[44]Max-Planck-Institut für Kernphysik, P.O. Box 103980, 69029 Heidelberg, Germany

[45]Friedrich-Alexander-Universität Erlangen-Nürnberg, Erlangen Centre for Astroparticle Physics, D 91058 Erlangen, Germany

ABSTRACT

The Cherenkov Telescope Array (CTA) is the next-generation ground-based observatory for very-high-energy gamma rays. One candidate design for CTA's medium-sized telescopes consists of the Schwarzschild-Couder Telescope (SCT), featuring innovative dual-mirror optics. The SCT project has built and is currently operating a 9.7-m prototype SCT (pSCT) at the Fred Lawrence Whipple Observatory (FLWO); such optical design enables the use of a compact camera with state-of-the art silicon photomultiplier detectors. A partially-equipped camera has recently successfully detected the Crab Nebula with a statistical significance of 8.6 standard deviations. A funded upgrade of the pSCT focal plane sensors and electronics is currently ongoing, which will bring the total number of channels from 1600 to 11328 and the telescope field of view from about 2.7° to 8°. In this work, we will describe the technical and scientific performance of the pSCT.

Keywords: Imaging Cherenkov Telescopes, Aplanatic Optical System, Gamma rays, Silicon photomultipliers, Schwarzschild-Couder Telescope

Send correspondence to Massimo Capasso capasso@nevis.columbia.edu

1. INTRODUCTION

Ground-based very-high-energy (VHE, E $>\sim$ 100 GeV) gamma-ray astronomy is a relatively young and yet powerful field of study, that allows us to probe the most energetic and explosive phenomena of the Universe. Because of the opacity of Earth's atmosphere at such energies, the detection of gamma rays on the ground is performed by indirect means. Photons entering the atmosphere degrade their energy through pair production and Bremsstrahlung losses, leading to the development of so-called electromagnetic (e.m.) *showers* (see e.g.:[1] for a schematic model of such a process). The charged particles in the shower travel faster than light's phase velocity in the atmosphere and the air molecules polarized by their passage emit radiation in a coherent wave.[2] Such radiation, also known as *Cherenkov* light, peaks at ultra-violet (UV) wavelengths and is emitted at very small angles ($\sim 1°$), so that an e.m. shower illuminates on the ground a *pool* of roughly 250 m diameter. Imaging Atmospheric Cherenkov Telescopes (IACTs) reconstruct images of e.m. showers to obtain the direction and energy of the original gamma ray, by means of a combination of a segmented-mirror reflector and a pixelated UV-sensitive camera with nanosecond sampling.[3]

From the pioneering experience of the Whipple 10 m telescope at the FLWO, that first detected VHE gamma-ray emission from the Crab Nebula,[4] IACTs have continuously improved, allowing physicists to unveil around 200 TeV emitters in both the Galactic and the extragalactic sky. Two of the three major IACTs currently operating (H.E.S.S[*] and VERITAS[†]) consist of arrays of IACTs with single-reflector telescopes implementing a Davies-Cotton (DC) design and with cameras based on photomultiplier tubes (PMTs); MAGIC[‡] features a parabolic reflector. Current DC designs, however, suffer from several limitations such as a relatively small field of view (FOV, $\sim 3.5° - 5°$) and a poor image resolution ($\sim 0.1°$[5]). Moreover, the image quality of DC-IACTs is further limited by comatic aberrations.[6] The Schwarzschild-Couder telescope (SCT) aims to overcome these limitations, with an aberration-free, wide FOV ($\sim 8°$) dual-mirror design.[7] The SCT is a candidate design for medium-sized telescopes (MSTs) of the Cherenkov Telescope Array (CTA), the next-generation ground-based observatory for VHE gamma rays.[8]

2. THE SCHWARZSCHILD-COUDER TELESCOPE: BIG EYES WITH A SHARPER VIEW.

The advantage of the SCT design is the correction of both comatic and spherical aberrations while retaining a large FOV.[9] An additional advantage of the dual-mirror structure is the possibility to focus the Cherenkov light on a smaller plate scale than existing IACTs. This opportunity enables the use of state-of-the-art solid-state sensors, i.e. silicon photomultipliers (SiPMs) to build a higher-resolution camera. Monte Carlo studies comparing the performance of DC- and SC-MST can be found here.[10] Figure 1 exemplifies the above-mentioned SCT advantages, by showing the improvement in the camera images of a gamma-ray- and a proton-induced shower, when moving from a classical DC to a SC design. In the following paragraphs, we will describe the two main components of the SCT: the optics and the focal plane.

2.1 Optical system components and performance

Figure 2 shows the structure of the optical system (OS) of the SCT. The primary reflector (M1) has a diameter of 9.7 m and is segmented in 48 panels, arranged in 2 concentric rings (32 outer primary - P2s and 16 inner primary - P1s); the secondary (M2) has a similar configuration (16 outer secondary - S2s and 8 inner secondary - S1s) and a diameter of 5.4 m. The de-magnifying M2 allows for a reduction of the effective optical system focal length of a factor of almost 3, if compared to DC-MSTs; the plate scale is hence reduced as well (1.625 mm/arcmin).

Each panel is equipped with a Stewart platform that allows for positioning with six degrees of freedom, mirror-panel edge sensors (MPES) for relative position monitoring, and a controller board. In order to achieve and maintain the alignment of such a complex mirror structure, both single-panel and global control systems are required. More specifically, the *panel-to-panel* alignment system (P2PAS) monitors and corrects for the relative displacement of pairs of adjacent segments. The *global alignment system*, instead, is composed of two optical

---

[*] https://www.mpi-hd.mpg.de/hfm/HESS/
[†] https://veritas.sao.arizona.edu/
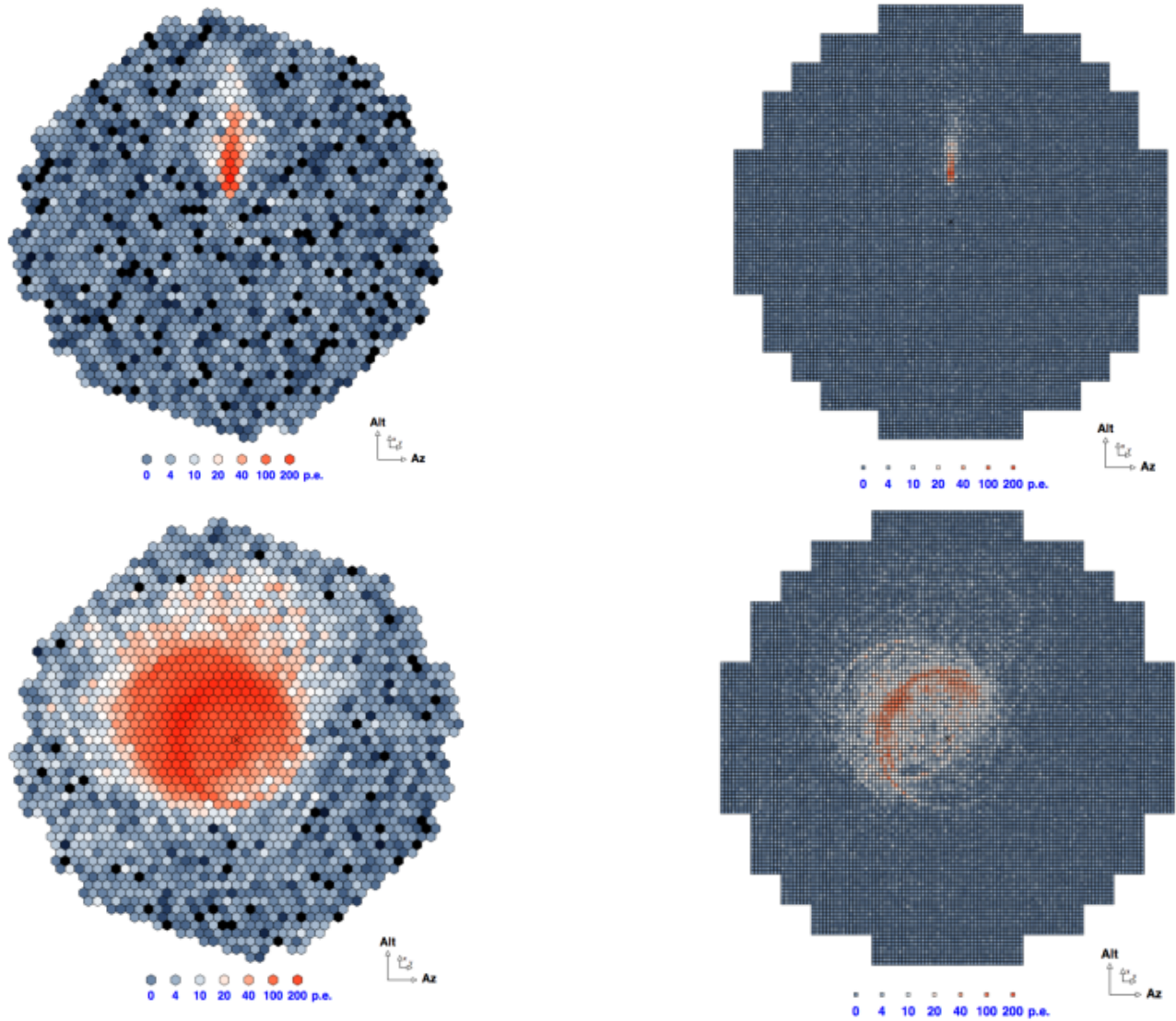[‡] https://magic.mpp.mpg.de/

Figure 1. From top left to bottom right: images of 1 TeV gamma-ray-induced showers (100 m impact distance), as seen by a standard DC-MST (top left) and a SC-MST camera (top right); images of 3.16 TeV proton-induced showers (0 m impact distance), as seen by a standard DC-MST (bottom left) and a SC-MST (bottom right) camera.
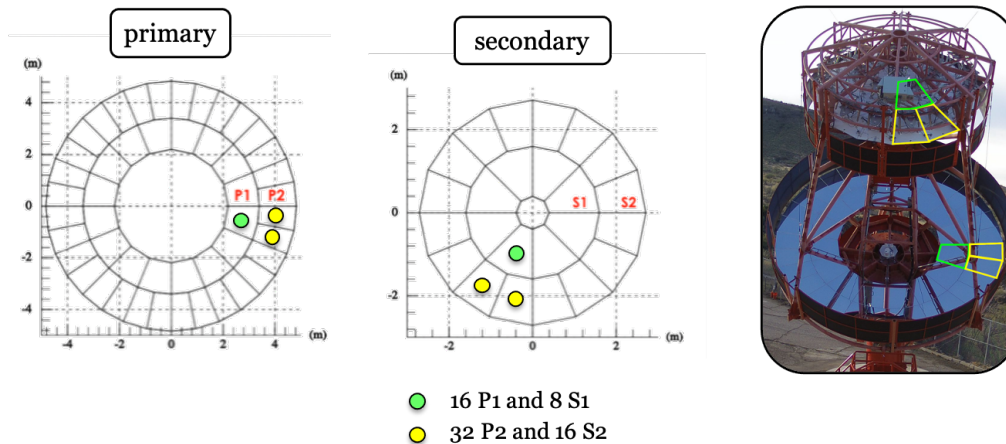
Figure 2. Structure of the SCT optics. Both the primary and secondary reflectors are composed by two concentric rings of aspheric panels. Figure adapted from[11] and.[9]

tables on M1 and M2, and the *optical camera alignment module* (OCAM), which can be installed in the focal plane replacing the central SiPM-camera focal plane module (FPM).

The optical point spread function (PSF) of the system is defined as $2 \times \max\{\sigma_\mathrm{x}, \sigma_\mathrm{y}\}$, where $\sigma_\mathrm{x}, \sigma_\mathrm{y}$ are the root mean square values on two orthogonal axes of the PSF. The *acceptable* and *goal* PSF are 3.2 arcmin and 2.6 arcmin, respectively. The alignment procedure exploits the de-focused images of stars to unambiguously identify the position of each panel; with this procedure, an on-axis PSF of 2.8 arcmin was achieved in December 2019 (see Figure 3 (left)). The details of the SCT OS components and its verification are described in.[9]
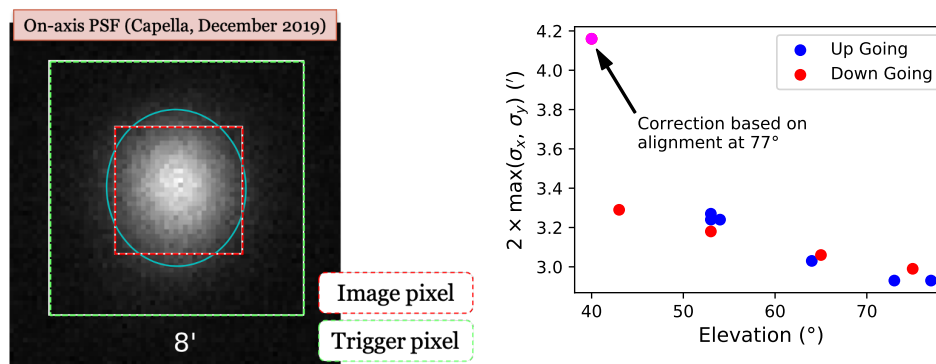

Figure 3. *Left*: Image of the star Capella on the SCT focal plane, after the alignment of the OS achieved in 2019. Highlighted in red and green are the SiPM-camera image (4 arcmin) and trigger (8 arcmin) pixel sizes. The cyan circle represents the 80% containment, as obtained from a 2D Gaussian fit. Image adapted from.[9] *Right*: Dependence of the optical PSF on telescope elevation. Image taken from.[12] Blue points correspond to elevations taken before the star culmination, red points to elevations taken afterwards.

The procedure followed in[9] was designed to align S2, P2 and P1 panels with respect to S1s (kept fixed). A separate procedure for S1-S1 alignment was developed and recently tested[12] during dedicated optics commissioning work in April 2021. In addition to the development of the S1-S1 alignment procedure, the dependence of the optical PSF on the telescope elevation was characterized. As already mentioned, the alignment procedure exploits the de-focused images of stars in the focal plane (see[9,12] for a detailed description). When everything is aligned, the image of the star is a point in the focal plane; by tilting P1s and P2s, while keeping S1s and S2s fixed, the point is split into two concentric rings (outer from P2s-S2s reflections, inner from P1s-S1s reflections); finally, by tilting S2s, a third intermediate ring is created. When the rings are aligned, the actuators' state is

saved in a database and the PSF for this configuration (after collapsing the rings back into focus) is calculated. As the measurements plotted on Figure 3 (right) show, an average PSF of about 3 arcmin across the tested range was achieved. At 40° elevation, the panel corrections as calculated for an elevation of 77° were used; this was deliberately done to estimate the effect of a poor alignment on the PSF. Along with making clear why an elevation-dependent panel alignment is needed, the measurement at 40° shows the stability of the OS, as the degraded PSF is only ∼15% higher than the acceptable PSF. We are currently planning to carry out more test campaigns, which will also be dedicated to perform measurements of the off-axis optical PSF performance, in order to provide a complete characterization of the SCT OS.

2.2 Focal plane

As mentioned in Section 2.1, the de-magnification achieved with the M2 reflector is such as to enable a reduced plate scale (78 cm diameter) with respect to conventional single-mirror MSTs (2.23 m diameter). Thanks to this, a much more finely pixelated camera (0.067° imaging pixel), based on silicon photomultipliers, can be employed. Over the past decade, SiPMs have reached a technological maturity such that they have been extensively used as a replacement for standard PMTs in applications where light detection to a single-photon level is required. Compact, rugged, and insensitive to magnetic fields, they come in different form factors (1 mm to 1 cm linear size) and spectral responses, for sensitivities optimized from vacuum- to near-ultraviolet (VUV/NUV)[13,14] to visible[15] to near-infrared (NIR).[16]

The SCT focal plane has a modular structure: it is divided into 9 sectors, each with the capability of housing up to 25 focal plane modules (FPMs). Each FPM consists of 64 6×6 mm^2 imaging pixels, for a total of 11328 pixels distributed over 177 FPMs (see[17] and references therein). The prototype SCT is currently populated with the central sector only and features a combination of SiPMs from 2 different manufacturers: 15 modules are based on Hamamatsu's S12642-0404PA-50(X) and 9 on Fondazione Bruno Kessler's NUV-HD (the central FPM slot is occupied by an OS calibration unit), for a total of 1536 pixels.

Groups of 4 neighboring image pixels (called a trigger pixel) are monitored for a threshold crossing of their analog sum. When 3 adjacent trigger pixels trigger in coincidence a camera trigger is produced (each trigger pulse is 10 ns wide and a 1.5 ns overlap between pulses is sufficient to generate a coincidence). A custom backplane handles camera triggers, along with power management and housekeeping. The analog signals from each FPM are sent to a front-end electronics (FEE) board through Samtec cables. The FEE houses preamplifiers and current sensors, as well as the TARGET 7 (7th generation of the *TeV Array Readout with GSa/s sampling and Event Trigger*[18–20]) digitizer and trigger chip. Figure 4 shows the components of a full module (FPM+FEE) of the pSCT.
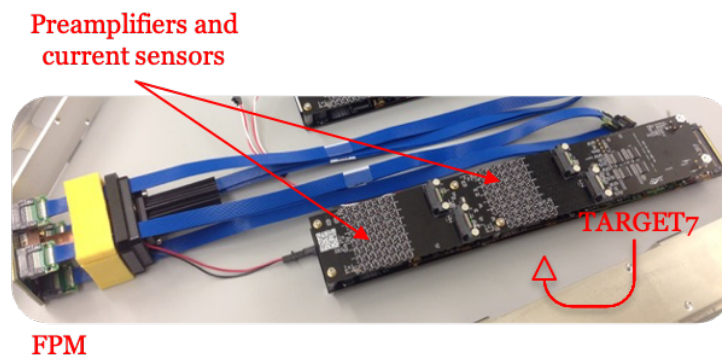

Figure 4. Components of a full module (FPM+FEE) of the pSCT.

3. SCT OPERATIONS

The construction of the pSCT began in June 2015 and first light operations (or observations) were achieved in January 2019. Since then, the SCT project has reached several important milestones. Of notable significance are

the achievement of the pre-construction estimated on-axis PSF (December 2019) and the detection of the Crab Nebula after the early 2020 data taking campaign. This detection was first announced during the 236th meeting of the American Astrophysical Society (May 2020) and recently published.[17] During the last year, despite the COVID-19 pandemic restrictions, we have continued technical work on both the OS (as described in Section 2.1) and the camera.

3.1 Observations of the Crab Nebula

The pSCT Crab Nebula campaign took place between January 18, 2020 and February 26, 2020 and is thoroughly described in.[17] In this section, we will outline the key points of the observation strategy, data analysis and results.

The observations on the Crab Nebula were performed in an ON/OFF (OFF/ON) mode: 28 minutes ON (OFF), 2 minutes slew, 28 minutes OFF (ON). The OFF pointing was offset in right ascension (RA) to ensure the same altitude-azimuth tracking coverage as for the on-source pointing. The deadtime-corrected ON and OFF exposures are 21.6 and 17.6 hours, respectively; 4 hour-long runs were taken in ON only mode, one of which was excluded and the remaining 3 used for calibration. The analysis was based on the Hillas parametrization of images of shower candidates[21] in the camera (*moment analysis*). The cuts on the Hillas parameters were derived from observations conducted simultaneously with the VERITAS array.[22] More specifically, coincident air shower events (including 18 candidate gamma rays in VERITAS) were utilized to optimize the cuts that separate gamma rays from cosmic-ray-induced showers in the pSCT dataset.

In addition to the Hillas analysis, we developed an offline pointing correction procedure using bright stars in the images of the SiPM current readings. Figure 5 (top) shows one of the images, with the center of the FOV and actual position of the Crab Nebula after alignment between the currents and star positions (in camera coordinates) for the time at which the reading was taken. Both Zeta Tau and O Tau are clearly visible in the Crab FOV and can be exploited (along with less bright stars) for alignment.

Ultimately, the signal from the Crab Nebula was detected with a significance of more than 8 standard deviations. Figure 5 (bottom) shows the distribution of the alpha parameter (the angle between the shower image major axis and the line connecting the image centroid to the Crab location) for both ON and OFF events. A clear excess towards the direction of the Crab nebula can be observed.

3.2 Technical work in the 2021 season

Following a ~3-month shutdown of FLWO, commissioning work on the SCT resumed in mid-2020, including efforts on both the optics and prototype camera, despite the global COVID-19 pandemic. One of the major improvements resulting from the work on the camera was the inclusion of FBK-SiPM-based modules in the trigger (they were excluded during the Crab campaign). Figure 6 (left) shows a block diagram of the trigger circuit schematic of TARGET 7 for one of the trigger groups. The signal from each channel is fed to two inverting amplifiers and then summed in groups of four with a summing inverting amplifier, with *PMTref4* as a reference voltage. This analog sum is fed to a comparator; lower values of the *thresh* parameter correspond to higher physical signals, while higher values eventually get into the baseline noise level. From laboratory measurements, we know that the range of linearity for the output of the summing amplifier (Node C) is 0.4-2.1 V. The PMTref4 value for each trigger pixel was initially tuned to have Node C set to 1.25 V for a baseline input, in order to accommodate for bi-polar signals. However, due to the fact that our signals are unidirectional, this choice effectively halved our dynamic range. Also, given that FBK and Hamamatsu SiPMs have different gains, this sub-optimal choice led to the former immediately reaching the noise level, rendering a trigger including all camera modules impossible to perform. We then changed Node C (and accordingly the tuning of PMTref4) to recover the *lost* half of the dynamic range. On the right side of Figure 6, the effect of such a modification is clearly visible. This plot shows the trigger rate as a function of the comparator value in the trigger line (at a constant rate of the flasher units that are installed on the secondary). Before the PMTref4 tuning, a high rate of noise triggers occurs for most thresholds (blue curve), while now (red curve) we have some room to perform a stable trigger on the signal at different amplitudes. As mentioned in,[17] the relatively low cosmic-ray rate (of few Hz) is due to the high threshold adopted to trigger the prototype camera above the electronic noise; for this reason, the *trigger scan* plot shown in Figure 6 appears dominated by flasher events.
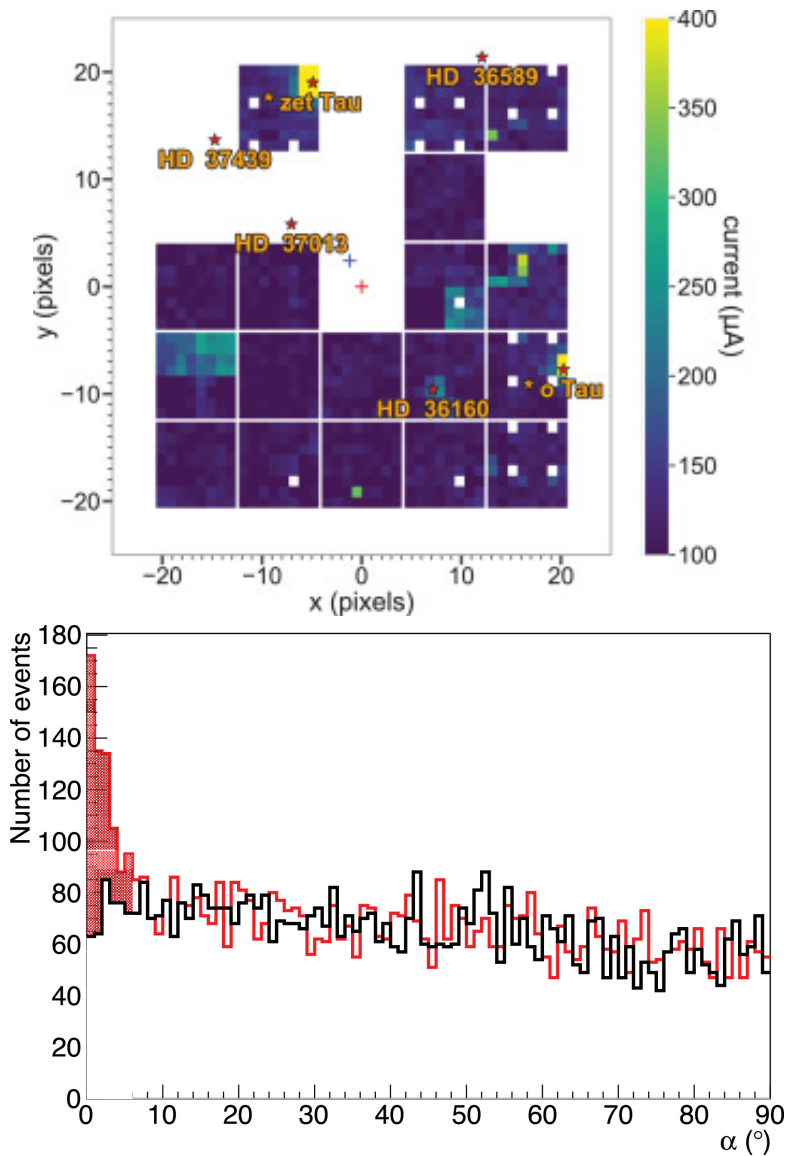
Figure 5. *Top*: Image from a current reading taken during an ON run. White pixels and modules are excluded due to hardware problems. Both Zeta Tau and O Tau are clearly visible in the Crab FOV and can be exploited (along with less bright stars) for alignment. The red cross marks the center of the FOV, while the blue cross marks the actual position of the Crab after correction. Figure taken from.[17] *Bottom*: ON (red) and OFF (black) events alpha histograms for the Crab dataset. Image taken from.[17]

4. TOWARDS THE CAMERA UPGRADE

The current prototype camera has several obvious limitations. The first one is its limited field of view (2.7°) with respect to the one of the fully populated focal plane (8°). The second is the noise of the current electronics implementation, which mainly stems from the relatively long distance between the sensors and pre-amplifying chain and the fact that the trigger and data paths are housed in the same chip. The currently ongoing camera upgrade aims to overcome these problems by adopting a single sensor type (FBK NUV-HD), new pre-amplifiers (SMART - SiPM Multichannel ASIC for high Resolution Cherenkov Telescopes), and an implementation of TARGET in which the digitization and trigger are performed by separate chips. Figure 7 shows laboratory measurements of the charge spectra for one full module under pulsed illumination, for the current implementation
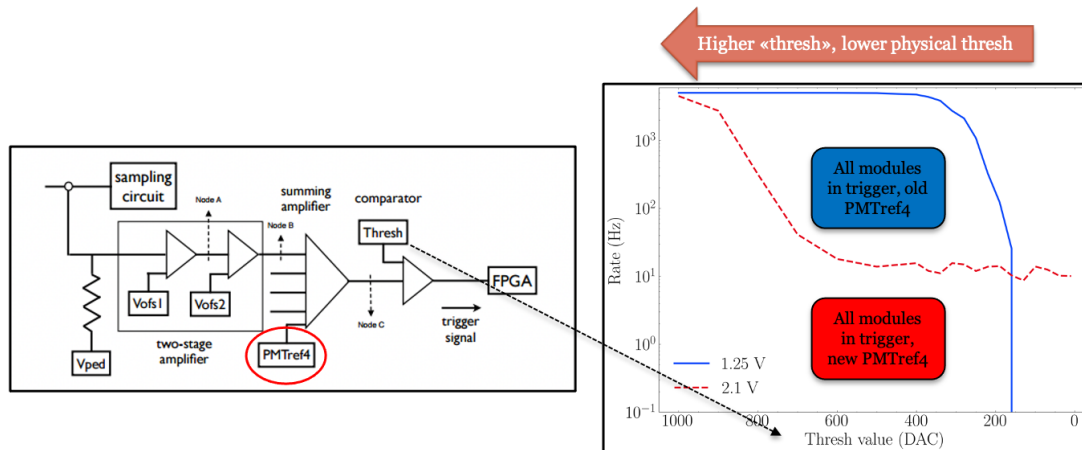
Figure 6. *Left*: Block diagram of the TARGET 7 trigger line, for one trigger pixel. *Right*: Rate scan as a function of *thresh*, at a constant flasher rate, before (blue curve) and after (red curve) PMTref4 adjustement. Image adapted from.[23]

of the electronics and the one foreseen for the upgrade; the adopted improvements lead to a dramatic recovery of the expected SiPM resolution. The details of the camera upgrade project will be given in a separate paper from this conference series Paper 11838-35.
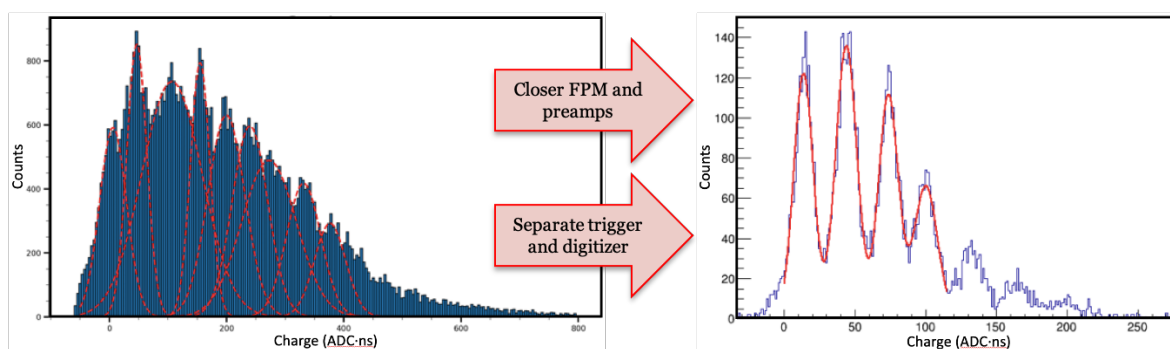

Figure 7. *Left*: Charge spectrum from one module mounting Hamamatsu SiPMs from the pSCT camera, under pulsed illumination. *Right*: Charge spectrum from one of the upgraded camera FPM+pre-amplifier+FEE assemblies, mounting FBK NUV-HD SiPMs. Image adapted from.[23]

5. CONCLUSIONS AND OUTLOOK

The Schwarzschild-Couder Telescope is an innovative dual-mirror prototype for the medium-sized contribution to CTA. During the last two years, the major technological challenges related to the OS design and an innovative camera based on solid-state sensors have been met. In this sense, the detection of the standard TeV source, the Crab Nebula, is of paramount significance for the SCT technology. It demonstrates the functionality of such an innovative IACT and offers proof of principle. The ongoing camera upgrade aims to overcome the current performance limitations, while fully populating the SCT field of view.

6. ACKNOWLEDGMENTS

REFERENCES

[1] Matthews, J., "A Heitler model of extensive air showers," *Astroparticle Physics* **22**, 387–397 (Jan. 2005).

[2] Grieder, P. K. F., [*Extensive Air Shower*], High Energy Phenomena and Astrophysical Aspects (2010).

[3] Völk, H. J. and Bernlöhr, K., "Imaging very high energy gamma-ray telescopes," *Experimental Astronomy* **25**, 173–191 (Aug. 2009).

[4] Weekes, T. C., Cawley, M. F., Fegan, D. J., Gibbs, K. G., Hillas, A. M., Kowk, P. W., Lamb, R. C., Lewis, D. A., Macomb, D., Porter, N. A., Reynolds, P. T., and Vacanti, G., "Observation of TeV Gamma Rays from the Crab Nebula Using the Atmospheric Cerenkov Imaging Technique," **342**, 379 (July 1989).

[5] Vassiliev, V. and Fegan, S., "High energy all sky transient radiation observatory," *arxiv.org/abs/astro-ph/0511342* (2005).

[6] Vassiliev, V. V., Fegan, S., and Brousseau, P., "Schwarzschild-couder two-mirror telescope for ground-based gamma-ray astronomy," *arxiv.org/abs/0708.2741* (2007).

[7] Vassiliev, V., Fegan, S., and Brousseau, P., "Wide field aplanatic two-mirror telescopes for ground-based -ray astronomy," *arxiv.org/abs/astro-ph/0612718v2* (2007).

[8] Cherenkov Telescope Array Consortium, T., :, Acharya, B. S., Agudo, I., Samarai, I. A., Alfaro, R., Alfaro, J., Alispach, C., Alves Batista, R., Amans, J.-P., and et al., "Science with the Cherenkov Telescope Array," *ArXiv e-prints* (Sept. 2017).

[9] Adams, C., Alfaro, R., Ambrosi, G., Ambrosio, M., Aramo, C., Benbow, W., Bertucci, B., Bissaldi, E., Bitossi, M., Boiano, A., Bonavolontà, C., Bose, R., Brill, A., Buckley, J. H., Byrum, K., Cameron, R. A., Capasso, M., Caprai, M., Covault, C. E., Venere, L. D., Fegan, S., Feng, Q., Fiandrini, E., Furniss, A., Garczarczyk, M., Garfias, F., Gent, A., Giglietto, N., Giordano, F., González, M. M., Halliday, R., Hervet, O., Hughes, G., Humensky, T. B., Ionica, M., Iriarte, A., Jin, W., Kaarat, P., Kieda, D., Kim, B., Licciulli, F., Limon, M., Loporchio, S., Masone, V., Meures, T., Mode, B. A. W., Mukherjee, R., Nieto, D., Okumura, A., Otte, N., Palombara, N. L., Pantaleo, F. R., Paoletti, R., Pareschi, G., Petrashyk, A., Powell, J., Powell, K., Ribeiro, D., Roache, E., Rousselle, J., Rugliancich, A., Ruíz-Díaz-Soto, J., Santander, M., Schlenstedt, S., Scuderi, S., Shang, R., Sironi, G., Stevenson, B., Stiaccini, L., Taylor, L. P., Tosti, L., Tovmassian, G., Vagelli, V., Valentino, M., Vandenbroucke, J., Vassiliev, V. V., Wakely, S. P., Wilcox, P., Williams, D. A., and Yu, P., "Verification of the optical system of the 9.7-m prototype Schwarzschild-Couder Telescope," in [*Optical System Alignment, Tolerancing, and Verification XIII*], Sasián, J. and Youngworth, R. N., eds., **11488**, 10 – 28, International Society for Optics and Photonics, SPIE (2020).

[10] Wood, M., Jogler, T., Dumm, J., and Funk, S., "Monte carlo studies of medium-size telescope designs for the cherenkov telescope array," *Astroparticle Physics* **72**, 11–31 (Jan 2016).

[11] Rousselle, J., Byrum, K., Cameron, R., Connaughton, V., Errando, M., Griffiths, S., Guarino, V., Humensky, T. B., Jenke, P., Kaaret, P., Kieda, D., Limon, M., Mognet, I., Mukherjee, R., Nieto, D., Okumura, A., Peck, A., Petrashyk, A., Ribeiro, D., Stevenson, B., Vassiliev, V., and Yu, P., "Toward the construction of a medium size prototype Schwarzschild-Couder telescope for CTA," in [*Optics for EUV, X-Ray, and Gamma-Ray Astronomy VII*], O'Dell, S. L. and Pareschi, G., eds., **9603**, 30 – 41, International Society for Optics and Photonics, SPIE (2015).

[12] Ribeiro, D., "Prototype schwarzschild-couder telescope for the cherenkov telescope array: Commissioning the optical system," in [*these proceedings*], PoS (ICRC2021) 717 (2021).

[13] Capasso, M., Acerbi, F., Borghi, G., Ficorella, A., Furlan, N., Mazzi, A., Merzi, S., Mozharov, V., Regazzoni, V., Zorzi, N., Paternoster, G., and Gola, A., "FBK VUV-sensitive Silicon Photomultipliers for cryogenic temperatures," *Nuclear Instruments and Methods in Physics Research A* **982**, 164478 (Dec. 2020).

[14] Gola, A., Acerbi, F., Capasso, M., Marcante, M., Mazzi, A., Paternoster, G., Piemonte, C., Regazzoni, V., and Zorzi, N., "Nuv-sensitive silicon photomultiplier technologies developed at fondazione bruno kessler," *Sensors* **19**(2) (2019).

[15] Piemonte, C., Ferri, A., Gola, A., Pro, T., Serra, N., Tarolli, A., and Zorzi, N., "Characterization of the first fbk high-density cell silicon photomultiplier technology," *IEEE Transactions on Electron Devices* **60**(8), 2567–2573 (2013).

[16] Acerbi, F., Paternoster, G., Gola, A., Zorzi, N., and Piemonte, C., "Silicon photomultipliers and single-photon avalanche diodes with enhanced nir detection efficiency at fbk," *Nuclear Instruments and Methods in Physics Research Section A: Accelerators, Spectrometers, Detectors and Associated Equipment* **912**, 309–314 (2018). New Developments In Photodetection 2017.

[17] Adams, C., Alfaro, R., Ambrosi, G., Ambrosio, M., Aramo, C., Arlen, T., Batista, P., Benbow, W., Bertucci, B., Bissaldi, E., Biteau, J., Bitossi, M., Boiano, A., Bonavolontà, C., Bose, R., Bouvier, A., Brill, A., Brown, A., Buckley, J., Byrum, K., Cameron, R., Canestrari, R., Capasso, M., Caprai, M., Covault, C., Depaoli, D., Errando, M., Fegan, S., Feng, Q., Fiandrini, E., Foote, G., Fortin, P., Funk, S., Furniss, A., Garfias, F., Gent, A., Giglietto, N., Giordano, F., Giro, E., González, M., Guarino, V., Halliday, R., Hervet, O., Holder, J., Hughes, G., Humensky, T., Ionica, M., Iriarte, A., Jin, W., Johnson, C., Kaaret, P., Kieda, D., Kim, B., Kuznetsov, A., Lapington, J., Licciulli, F., Loporchio, S., Masone, V., Meagher, K., Meures, T., Mode, B., Mognet, S., Mukherjee, R., Nguyen, T., Nieto, D., Okumura, A., Otte, N., La Palombara, N., Pantaleo, F., Paoletti, R., Pareschi, G., Petrashyk, A., Di Pierro, F., Pueschel, E., Reynolds, P., Ribeiro, D., Richards, G., Roache, E., Ross, D., Rousselle, J., Rugliancich, A., Ruíz-Díaz-Soto, J., Santander, M., Schlenstedt, S., Schneider, M., Scuderi, S., Shang, R., Sironi, G., Stevenson, B., Stiaccini, L., Tajima, H., Taylor, L., Thornhill, J., Tosti, L., Tovmassian, G., Vagelli, V., Valentino, M., Vandenbroucke, J., Vassiliev, V., Di Venere, L., Wakely, S., Watson, J., White, R., Wilcox, P., Williams, D., Wood, M., Yu, P., and Zink, A., "Detection of the crab nebula with the 9.7 m prototype schwarzschild-couder telescope," *Astroparticle Physics* **128**, 102562 (2021).

[18] Bechtol, K., Funk, S., Okumura, A., Ruckman, L., Simons, A., Tajima, H., Vandenbroucke, J., and Varner, G., "Target: A multi-channel digitizer chip for very-high-energy gamma-ray telescopes," *Astroparticle Physics* **36**(1), 156–165 (2012).

[19] Tibaldo, L., Vandenbroucke, J. A., Albert, A. M., Funk, S., Kawashima, T., Kraus, M., Okumura, A., Sapozhnikov, L., Tajima, H., Varner, G. S., Wu, T., and Zink, A., "Target: toward a solution for the readout electronics of the cherenkov telescope array," (2015).

[20] Albert, A., Funk, S., Katagiri, H., Kawashima, T., Murphy, M., Okumura, A., Quagliani, R., Sapozhnikov, L., Shigenaka, A., Tajima, H., Tibaldo, L., Vandenbroucke, J., Varner, G., and Wu, T., "Target 5: A new multi-channel digitizer with triggering capabilities for gamma-ray atmospheric cherenkov telescopes," *Astroparticle Physics* **92**, 49–61 (2017).

[21] Hillas, A. M., "Cerenkov Light Images of EAS Produced by Primary Gamma Rays and by Nuclei," in [*19th International Cosmic Ray Conference (ICRC19), Volume 3*], *International Cosmic Ray Conference* **3**, 445 (Aug. 1985).

[22] Park, N., "Performance of the VERITAS experiment ," in [*Proceedings of The 34th International Cosmic Ray Conference — PoS(ICRC2015)*], **236**, 771 (2016).

[23] Taylor, L. P., "Design and performance of the prototype schwarzschild-couder telescope camera," in [*these proceedings*], PoS (ICRC2021) 748 (2021).